AIAA Guidance, Navigation and Control Conference and Exhibit
18 - 21 August 2008, Honolulu, Hawaii

AIAA 2008-6515

An Optimal Strategy for Persistent Contrail Avoidance

Scot E. Campbell[1], Natasha A. Neogi[2], and Michael B. Bragg[3]
University of Illinois Urbana-Champaign, Urbana, IL, 61801

Persistent contrails have been recognized as a potential threat to the global climate. This paper presents a methodology to optimally reroute aircraft trajectories to avoid the formation of persistent contrails with the use of mixed integer programming (MIP). The main contributions of this paper are the introduction of a more realistic fuel burn model, and the implementation of a quadratic cost function. Existing MIP path planning literature has used a 1-norm approximation of the vehicle acceleration for fuel burn. The fuel burn model created for this paper is based on aircraft data and engine performance software, and the fuel burn cost was approximated with piecewise linear, and quadratic functions for implementation into the MIP. Fuel optimal trajectories for contrail avoidance were created for each cost function and the results were compared. In addition, differences between the linear and quadratic cost were investigated with a pathological obstacle field, and the sensitivity of the trajectory to changes in the planning horizon length and time step size are presented. For a specific scenario, it was found that persistent contrails could be avoided with a 2.76% increase in fuel burn.

I. Introduction

AVIATION affects the environment through many different pathways including land use, noise pollution, local air quality, and climate.[1] Currently, its effect on climate is not fully understood,[1] but there are concerns that aircraft emissions might play a larger role in future global climate change.[2,3] The three largest aviation emissions effectors on the climate are direct emission of greenhouse gases such as CO_2, emissions of NOx, and persistent contrails.[2,3] In general, persistent contrails are formed when an aircraft passes through an ice-supersaturated region in the atmosphere. Although the complete effect of persistent contrails on the environment is not known, there is evidence to suggest an effect,[4] and it is predicted that persistent contrails have a three to four times greater effect on the climate than CO2 emissions.[1] With a projected three fold increase in air traffic by the year 2025,[5] the effect of aviation on the environment will increase with time. Recent research has investigated operational strategies to mitigate persistent contrail formation through air traffic management scenarios. These strategies include the restriction of cruise altitudes,[6-8] the real-time adjustment of cruise altitude,[9] and rerouting the flight plans of aircraft to avoid areas conducive to persistent contrail formation.[10] However, while these approaches might be effective, they do not seek the true optimal trajectory in terms of fuel cost and contrail avoidance.

Optimal trajectory planning has been investigated through many different techniques.[11-15] Mixed-integer programming (MIP) has been successfully applied to trajectory optimization problems involving constrained dynamics and obstacle avoidance using both full horizon, and receding horizon implementations.[14-21] One drawback to full horizon MIP is the optimization can be intractable for large problems, i.e. many obstacles, discrete time steps, dynamic constraints. To make large problems tractable, a receding horizon controller can be used to speed up the solution time.[16,17] A receding horizon controller essentially finds the optimal trajectory up to a certain point, called the planning horizon, and then approximates the remaining trajectory to the goal.[16] The controller executes a pre-specified number of time steps in the optimal trajectory and the optimization is iterated until the goal is reachable in the planning horizon.[16]

This paper will use MIP to find the fuel optimal trajectory of an aircraft flying from O'Hare International Airport (KORD) to Los Angeles International Airport (KLAX) while avoiding areas favorable to persistent contrail formation. Unlike previous papers using MIP to find fuel optimal trajectories,[19,20] this paper will use a more realistic fuel burn model developed from aircraft data and engine performance software. In addition, due to the nonlinear

[1] Graduate Research Assistant, Aerospace Engineering, AIAA Member.
[2] Assistant Professor, Aerospace Engineering, AIAA Member.
[3] Professor, Aerospace Engineering, Executive Associate Dean for Academic Affairs, AIAA Fellow.

nature of aircraft fuel burn, this paper will investigate the viability of mixed-integer quadratic programming (MIQP) as an alternative to the popular mixed-integer linear programming (MILP) problem formulation.

II. Contrail Formation and the Atmospheric Model

Contrails are line-shaped clouds that form behind aircraft at high-altitudes.[22] After forming, contrails dissipate if the relative humidity with respect to ice (RHi) is low, and persist if the RHi is high. The RHi threshold at which contrails persist is thought to vary between 95-105%,[23] but for simplicity, this paper used RHi > 100% to define the necessary condition for persistent contrail formation.

The Rapid Update Cycle (RUC) is an atmospheric prediction system that is principally a numerical forecast model developed for users needing short-range weather forecasts.[24] The RUC data have horizontal resolutions of 20km, 40km, and 60km, with 40km being used for this paper because it is the most accurate for contrail estimation.[10] The vertical resolution of the data are isobaric pressure levels ranging from 100-1000mb in 25mb increments. The RUC does not directly output RHi, but it can be calculated from the relative humidity with respect to water (RHw) and the environmental temperature. This paper used archived RUC data from November 17, 2001.

For MIP implementation, the areas of RHi > 100% were represented as overlapping cuboids. Figure 1 shows the November 23, 2000 field of RHi at different altitudes.

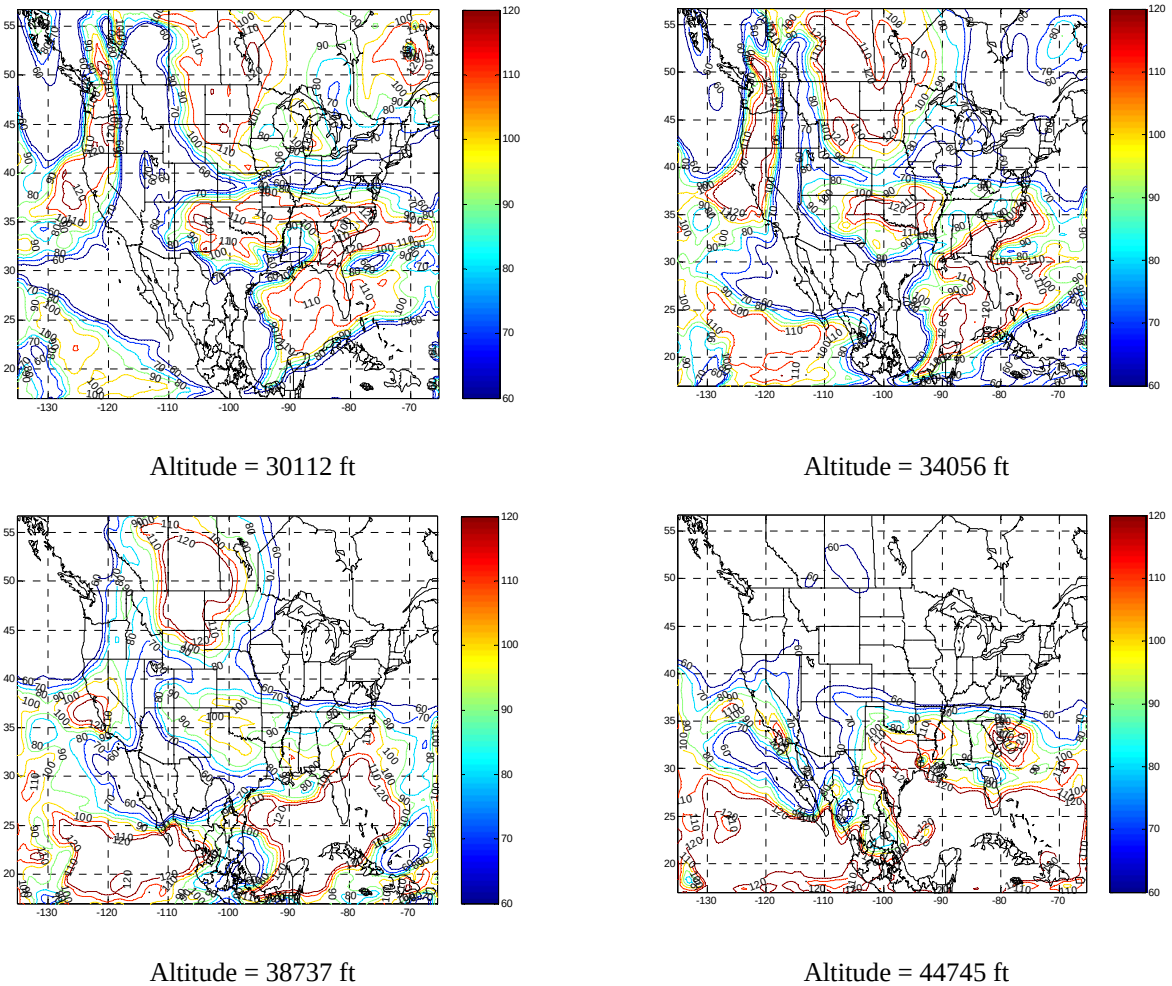

Fig. 1 Fields of RHi at Different Altitudes on November 23, 2000, RUC data.

Note that the corresponding altitudes to the RUC isobaric pressure levels were found using the standard atmosphere. Figure 2 shows the RHi field represented by a set of overlapping cuboids.

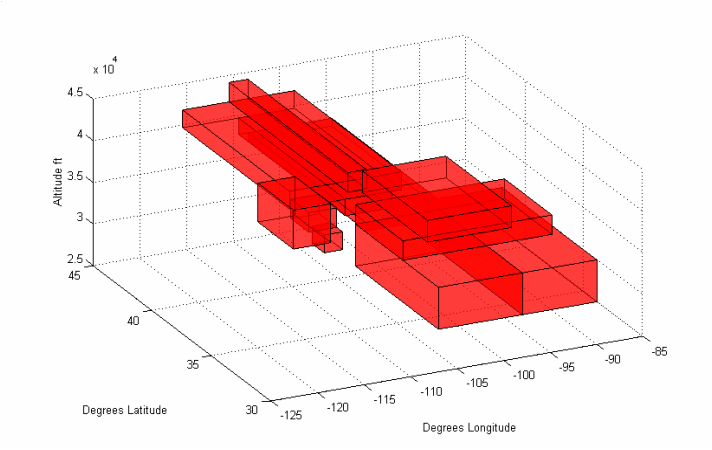

Fig. 2 Cuboid representation of RHi Field

III. Aircraft Fuel Burn Model

Aircraft fuel burn is a complicated quantity that is dependent on many states and aircraft-specific parameters. In practice, fuel burn is predicted based on flight test data taken over a wide range of operating conditions. In lieu of these data, fuel burn can be approximated with a limited set of aircraft and engine data. Previous studies have predicted fuel burn using the FAA's System for Assessing Global Emissions (SAGE),[10] a modified version of SAGE,[25] and a quadratic approximation based on velocity.[26] Existing work using the MILP framework have approximated fuel burn by the 1-norm of the aircraft acceleration.[19,20] This paper uses aircraft data and engine performance simulation software to approximate fuel burn over the cruise flight envelope. This method is better model than a 1-norm approximation or velocity approximation, but simple enough to implement in the mixed-integer programming framework.

A. Aircraft Performance

The aircraft performance model used for this paper was created to emulate the en-route performance characteristics of medium-range aircraft such as the Boeing 737 and Airbus A320. The following restrictions were placed on the altitude and Mach number to confine aircraft performance to the cruise envelope, as seen in Eq. (1)

$$\begin{aligned} 0.70 \le M \le 0.82 \\ 28{,}000\, ft \le z \le 42{,}000\, ft \end{aligned} \tag{1}$$

where M is the Mach number and z is the altitude. To compute the performance, the drag coefficient was extracted from drag polar data[27] for a range of Mach numbers, altitudes, and weights. The thrust required was calculated for the range of Mach numbers and altitudes given by Eq. (1) and for three weights, each representing the aircraft weight at a different fuel state along the flight path.

B. Engine Performance

Engine performance was obtained with the Engine Performance Analysis Program v4.2.[29] This program uses a set of engine parameter inputs and flight conditions (Mach number, altitude) to compute curves of thrust specific fuel consumption (TSFC) vs. engine thrust. The engine was assumed to be a high-bypass turbofan, and the software input parameters are given in Table 1.

Table 1 Engine Performance Software Input Parameters

Mass Flow Rate (max throttle, seal level)	779 lbm/sec
Bypass Ratio	5.1
Compressor Pressure Ratio	32.8
Fan Pressure Ratio	2.3

The program was run for the range of Mach numbers and altitudes given by Eq. (1). The engine performance data were tabulated for use in the aircraft fuel burn model.

C. Aircraft Fuel Burn

Aircraft fuel burn was calculated for a range of Mach numbers, altitudes, and weights using Eq. (2)

$$W_f = T_{req} \cdot TSFC \tag{2}$$

where W_f is the fuel flow, T_{req} was found by the aircraft performance calculations, and $TSFC$ was found by the engine performance model. Figures 3 and 4 show the relationship of altitude and velocity with fuel flow, respectively, for an aircraft weight of 145,000 lb with engine and drag characteristics described above.

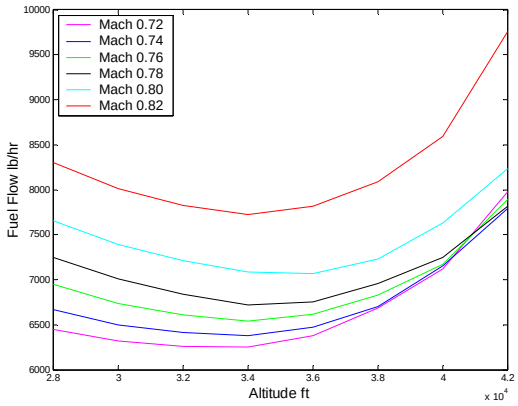

Fig 3. Altitude vs. Fuel Flow for W = 145,000 lb

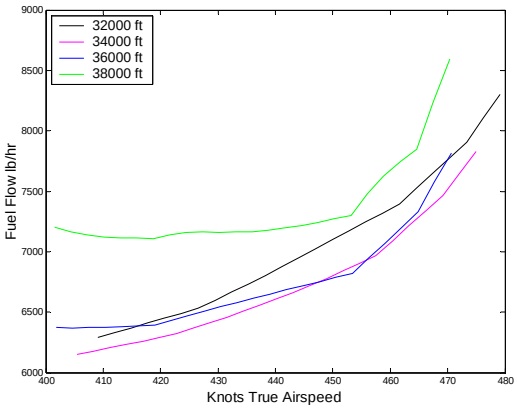

Fig 4. Velocity vs. Fuel Flow for W = 145,000 lb

Figures 3 and 4 show the highly nonlinear nature of fuel burn. To simplify this behavior, a nominal flight condition was selected (Mach number, altitude) for a given weight, and the change in fuel burn around the nominal flight condition was modeled. The nominal cruise Mach number was selected to be 0.78 based on typical cruise speeds for the type of aircraft considered in this model.[30] The nominal cruise altitude was selected based on the optimal altitude for a Mach number of 0.78 and for a given weight. Ideally, the nominal altitude would increase continuously as the weight of fuel is burned off of the aircraft, resulting in a cruise climb flight profile. However, this procedure is generally not performed in practice because of air traffic control restrictions. Instead, a step-climb procedure is used, where the altitude is increased in discrete steps along the flight path.[31] This model emulated a step climb by using three nominal cruise altitudes based on the optimal altitude for three aircraft weights. The initial weight was assumed to be 145,000 lbs, and the subsequent weights were 135,000 lbs and 125,000 lbs, which corresponded to optimal altitudes of approximately 34,000 ft, 36,000 ft, and 38,000 ft, respectively, for a Mach number of 0.78. Table 3 gives the nominal flight conditions used for this model.

Table 2 Nominal Flight Conditions

Weight (lb)	Altitude (ft)	Mach number	True airspeed (knots)
145,000	34,000	0.78	451
135,000	36,000	0.78	447
125,000	38,000	0.78	447

Figures 5 and 6 show the sensitivity of fuel flow to changes in altitude and velocity around the nominal flight conditions, respectively.

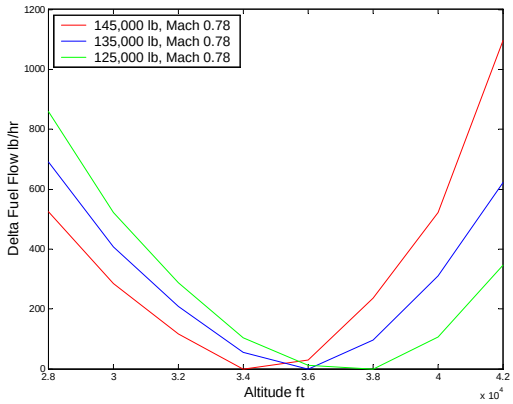

Fig. 5 Sensitivity of fuel flow to altitude

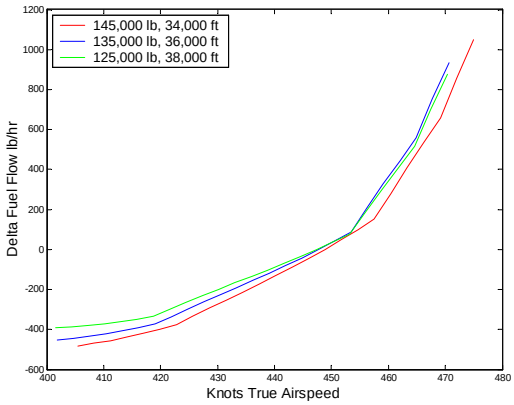

Fig. 6 Sensitivity of fuel flow to velocity

IV. MILP Receding Horizon Formulation

This section describes the formulation of the persistent contrail mitigation problem as a receding horizon mixed-integer linear program (RH-MILP). The general structure of the receding horizon controller follows from previously published work.[15,16] To summarize this work, the RH-MILP algorithm can be thought of in two parts: a detailed trajectory optimization with a pre-specified time horizon, followed by a less refined approximation of the cost from the end of the detailed trajectory to the goal. Once the detailed trajectory and approximate cost-to-go is optimized, a pre-specified number of time steps in the detailed trajectory are executed, and the optimization is recomputed with the updated initial condition. This procedure continues until the goal is reachable in the time horizon of the detailed trajectory, also called the planning horizon. This section will show the implementation of a more realistic aircraft fuel burn model within a general framework given by existing work in RH-MILP for trajectory optimization.[15,16] The optimizations were solved using CPLEX 10.2 on a laptop with a 2.16 GHz Intel Core2 Duo processor and 2 GB of RAM.

A. Aircraft Model Implementation – The Constraints

The detailed trajectory optimization phase of the receding horizon controller uses MILP to find the fuel optimal trajectory from an initial state to the end of the planning horizon. Previous studies investigated fuel optimal RH-MILP by approximating fuel burn by the 1-norm of the acceleration.[19,20] This paper provides a more realistic implementation of fuel burn and aircraft performance limits encountered in a high-altitude transonic cruise scenario.

The dynamical constraints presented here are that of a double integrator and the evolution of the aircraft states is governed by Eq. (5)

$$\mathbf{x}(k+1) = A\mathbf{x}(k) + b\mathbf{u}(k) \tag{5}$$

where,

$$\mathbf{x} = \begin{bmatrix} x \\ y \\ z \\ v_x \\ v_y \\ v_z \end{bmatrix} \qquad \mathbf{u} = \begin{bmatrix} a_x \\ a_y \\ a_z \end{bmatrix} \qquad A = \begin{bmatrix} I_3 & \Delta t \cdot I_3 \\ 0_3 & I_3 \end{bmatrix} \qquad b = \begin{bmatrix} \tfrac{1}{2}\Delta t^2 \cdot I_3 \\ \Delta t \cdot I_3 \end{bmatrix} \tag{6}$$

The vector **x** represents the position and velocity of the aircraft, the vector **u** represents the acceleration, k is the discrete time step, and Δt is the size of the time step.

The calculation of velocity magnitude from the individual velocity components requires the square root of the sum of the squares, which is obviously a nonlinear operation and inadmissible in MILP. Therefore an accurate

method is needed to approximate the magnitude of velocity because fuel burn is largely dependent on the speed of the aircraft. The following procedure provides a linear approximation of the velocity and the acceleration for implementation into the MILP[15]

$$V[k] \geq v_x[k]\cos\left(\frac{2\pi m}{M}\right) + v_y[k]\sin\left(\frac{2\pi m}{M}\right) \tag{7}$$

$$V[k] - R \cdot (1 - b_v[k,m]) \leq \left(v_x[k]\cos\left(\frac{2\pi m}{M}\right) + v_y[k]\sin\left(\frac{2\pi m}{M}\right)\right) \cdot 1.01 \tag{8}$$

$$A[k] \geq a_x[k]\cos\left(\frac{2\pi m}{M}\right) + a_y[k]\sin\left(\frac{2\pi m}{M}\right) \tag{9}$$

where V and A are the velocity and acceleration magnitudes respectively, b_v is a binary variable, R is a large constant, and m is an integer in the set of integers from 1 to M. Equation 8 is necessary to include non-convex constraints on minimum velocity. It should be noted here that the velocity and acceleration magnitude approximations only account for motion in the x-y direction. Motion in the z-direction was treated separately. Additionally, V and A were bounded to constrain the optimization within a realistic flight envelope, as given in Eqs. (9) and (10):

$$V_{\min} \leq V \leq V_{\max} \tag{9}$$

$$A \leq A_{\max} \tag{10}$$

The vertical velocity was constrained by a rate of climb limit, which was a function of the altitude. The maximum rate of climb was defined by Eq. (11)

$$RC_{\max} + \beta_1 z = \beta_0 \tag{11}$$

where RC_{max} is the maximum rate of climb, and β_i was computed in the aircraft model. The rate of climb was constrained by the maximum rate of climb using Eq. (12)

$$v_z - RC_{\max} \leq 0 \tag{12}$$

The maximum descent rate was represented by a lower bound on the vertical velocity and was chosen to be a value consistent with normal operation of commercial aircraft.[28]

Terminal constraints were used to encourage the aircraft to reach the goal if the goal was reachable in the planning horizon. These constraints use binary variables and are shown in Eqs. (13) and (14)

$$\begin{aligned}
x[k] + R \cdot b_f[k] &\leq R + x_f \\
x[k] + R \cdot b_f[k] &\leq R - x_f \\
y[k] + R \cdot b_f[k] &\leq R + y_f \\
y[k] + R \cdot b_f[k] &\leq R - y_f \\
z[k] + R \cdot b_f[k] &\leq R + z_f \\
z[k] + R \cdot b_f[k] &\leq R - z_f
\end{aligned} \tag{13}$$

$$\sum_{i=1}^{N_p} b_f[i] \le 1 \tag{14}$$

where $b_f[k]$ is the binary variable corresponding to time step k, (x_f, y_f, z_f) is the final position, and R is a large constant used to relax the constraint. In the literature, this approach is referred to as the "big-M" approach.

B. Aircraft Model Implementation – The Cost

As shown in section III, aircraft fuel burn is extremely nonlinear by nature, and in turn, difficult to implement in a linear structure. In a cruise flight condition, the main drivers of fuel burn are velocity, altitude, and weight. If climbing or descending, the throttle setting is also a factor. To reiterate the assumptions used in section III, the effect of Mach number, altitude, and throttle setting were assumed to be decoupled around a nominal flight condition and weight. Also, the effect of weight was accounted for by changing the nominal flight condition at pre-specified intervals of time, corresponding to the approximate time the aircraft becomes 135,000 lbs and 125,000 lbs during the flight. The fuel burn curves given in Figs. 5 and 6 were written as a set of piecewise linear functions. The piecewise linear representation of fuel burn as a function of weight is described by Eqs. (15) and (16):

$$f_a(W) = \max(\mu_1 z + \mu_2, ..., \mu_i z + \mu_{i+1}) \quad \text{for } i = 1,3,5,\ldots \tag{15}$$

$$f_v(W) = \max(\sigma_1 V + \sigma_2, ..., \sigma_i V + \sigma_{i+1}) \quad \text{for } i = 1,3,5,\ldots \tag{16}$$

where $f_a(W)$ and $f_v(W)$ are the fuel burn associated with altitude and velocity, respectively, W is weight, and μ_i and σ_i determine the piecewise linear function. These equations are written in MILP format as follows:

$$\begin{aligned} &\mu_1 z - f_a \le \mu_2 \\ &\quad\vdots \qquad\qquad \text{for } i = 1,3,5,\ldots \\ &\mu_i z - f_a \le \mu_{i+1} \end{aligned} \tag{17}$$

$$\begin{aligned} &\sigma_1 V - f_v \le \sigma_2 \\ &\quad\vdots \qquad\qquad \text{for } i = 1,3,5,\ldots \\ &\sigma_i V - f_v \le \sigma_{i+1} \end{aligned} \tag{18}$$

It should be noted that the coefficients μ and σ depend on the aircraft weight; therefore these equations are updated whenever the aircraft weight is updated.

The effect of climb and descent on fuel burn was assumed to be decoupled from the effects of velocity, altitude, and weight. During cruise, commercial aircraft frequently change altitude using the flight level change mode of the flight management system, and therefore it was assumed that the thrust is set to maximum climb thrust during climb, and idle during descent. The climb and descent state was characterized with Eq. (19)

$$\begin{aligned} v_z &\le R \cdot b_{climb} \\ -v_z &\le R \cdot b_{descend} \end{aligned} \tag{19}$$

where v_z is the vertical velocity, R is a large constant, b_{climb} is a binary variable to indicate climb, and $b_{descend}$ is a binary variable to indicate descent.

The last component of the cost is the fuel burn associated with acceleration, which is determined under the assumption that the fuel burn linearly increases with acceleration. In full, the cost function for the detailed trajectory optimization is written as Eq. (20)

$$J = \left(f_a + f_v + A\right)\Delta t - \sum_{i=1}^{N_p} b_{f,i} f_{term,i} + b_{climb,i} f_{descend} + b_{descend,i} f_{descend} \tag{20}$$

where f_a and f_v are the fuel cost associated with altitude and velocity, respectively, A is acceleration, f_{climb} is a weighting associated with maximum climb thrust, $f_{descend}$ is a weighting associated with idle, and Δt is the time step. Again, it should be noted that f_a and f_v change with aircraft weight, which is updated periodically during the receding horizon optimization.

C. Obstacle Avoidance Constraints

Obstacle avoidance is accomplished within the MILP framework by using n constraints to break the problem into n convex subproblems, which are solvable by linear programming. This identical procedure was used in some of the existing literature.[15,16,18] For simplicity, this paper only considered cuboid obstacles to represent areas of RHi greater than 100%. More complex regions were created with the intersection of multiple cuboids.

D. The Cost-to-Go

The detailed trajectory is planned until the end of the planning horizon, and the remaining trajectory to the goal is approximated by the cost-to-go function. The cost-to-go function approximates the fuel required to go from the end of the planning horizon to the goal by creating a cost map containing the fuel to travel from each node in the map to the goal, and an additional fuel cost to connect the detailed trajectory to the cost map.

The cost map, G_{ij}, is a measure of the cost between nodes i and j, and is found using a visibility graph weighted by the distance between nodes and a cost associated with the altitude of the nodes. The visibility graph was found with a linear program.[15]

To assign a realistic cost approximation to the visibility graph, it was weighted by a two part function. The first part approximates the fuel burn between the nodes based on the Euclidian distance between the nodes, and the second part is an altitude penalty based on a quadratic altitude function evaluated at the average altitude of the connecting nodes. Therefore, the cost to travel between nodes i and j is given by Eqs. (21) and (22)

$$G_{ij} = \lambda \left\| \mathbf{x}_i - \mathbf{x}_j \right\|_2 + \alpha_1 z_{avg}^2 + \alpha_2 z_{avg} + \alpha_3 \tag{21}$$

$$z_{avg} = \frac{1}{2}\left(z_i + z_j\right) \tag{22}$$

where z_{avg} is the average altitude of the connecting nodes, α_i is determined by the aircraft model, and λ is a constant used to transform distance to fuel burn. Dijkstra's Algorithm was applied to the cost map to find the path of minimum fuel cost from each node to the goal. The output is a vector, C_i, which gives the cost to go from each node i in the cost map to the goal.

The cost-to-go was completed by connecting the end of the detailed trajectory to a point in the cost map. The position at the end of the detailed trajectory, $\mathbf{x}[k+N_p]$, and the node in the cost map, $\mathbf{x}_{cp}$, are chosen by the optimization so that they are mutually visible and that the fuel cost required to travel between them is minimized. Visibility is ensured by requiring a set of interpolation points between $\mathbf{x}[k+N_p]$ and $\mathbf{x}_{cp}$ to remain outside of the obstacles defined in subsection C. Equation (23) is used to select the visible point

$$\begin{aligned} \sum_{i=1}^{n_{cp}} b_{vis,i} \mathbf{x}_{cp,i} &= \mathbf{x}_{vis} \\ \sum_{i=1}^{n_{cp}} b_{vis,i} &= 1 \end{aligned} \tag{23}$$

where $b_{vis,i}$ is a binary variable for cost point i, and n_{cp} is the number of nodes. The cost associated with traveling this path is a function of the Euclidian distance and the altitude of the interpolation points. The Euclidian distance, D, was approximated with Eq. (24)

$$D \geq \lambda\left(\Delta x \sin\left(\frac{2\pi m_1}{M_1}\right)\cos\left(\frac{2\pi m_2}{M_2}\right)+\Delta y \sin\left(\frac{2\pi m_1}{M_1}\right)\sin\left(\frac{2\pi m_2}{M_2}\right)+\Delta z \cos\left(\frac{2\pi m_1}{M_1}\right)\right)$$
$$m_i = 1...M_i \tag{24}$$
$$i \in [1,2]$$

where m_i is the set of integers between 1 and M_i, and Δx, Δy, and Δz are the distances between $\mathbf{x}[k+N_p]$ and $\mathbf{x}_{cp}$ in the x, y, and z direction, respectively. The altitude of the interpolation points was penalized using the same philosophy as in equation 17, which penalizes flight away from the optimal altitude. The complete cost-to-go function is given in Eq. (25)

$$J = C^T \cdot b_{vis} + \sum_{i=1}^{n_I} f_{x,i} + D \tag{25}$$

where C is the cost vector, f_x is the interpolation point altitude cost, n_I is the number of interpolation points, and D is the cost of flight between $\mathbf{x}[k+N_p]$ and $\mathbf{x}_{cp}$.

E. The Complete Cost Function

The complete cost function is the sum of Eqs. (22) and (27). This cost reflects the detailed cost in the planning horizon and the cost approximation from the cost-to-go function. Note that the cost-to-go and the detailed trajectory are not completely independent due to the fact that $\mathbf{x}[k+N_p]$ and $\mathbf{x}_{cp}$ are not chosen independently.

V. MIQP Receding Horizon Formulation

The RH-MILP was reformulated using receding horizon mixed-integer quadratic programming (RH-MIQP) because a quadratic cost is a better representation of the sensitivity of fuel burn to aircraft velocity and altitude, as is shown in section III. All of the dynamical constraints, as well as the cost-to-go approximation, were unchanged in this reformulation.

The cost function of the RH-MIQP formulation is similar to the RH-MILP formulation in that it is composed of a detailed trajectory cost and a cost-to-go. For this paper, only the detailed trajectory cost was reformulated as a quadratic function, the cost-to-go was left unchanged. The quadratic altitude and velocity costs were fit from the curves of Figs. 5 and 6, and take the form of Eqs. (26) and (27), respectively.

$$f_{Q,a}(W) = \eta_1 z^2 - \eta_2 z + \eta_3 \tag{26}$$

$$f_{Q,v}(W) = \eta_4 V^2 - \eta_5 V + \eta_6 \tag{27}$$

where $f_{Q,a}(W)$ and $f_{Q,v}(W)$ are the altitude and velocity costs, respectively, and η_i is taken from the aircraft model. Note that like in the RH-MILP formulation, $f_{Q,a}(W)$ and $f_{Q,v}(W)$ are updated when the aircraft weight changes. The sum of Eqs. (28) and (29) form the quadratic component of the cost function, which is shown graphically in Fig. 7.

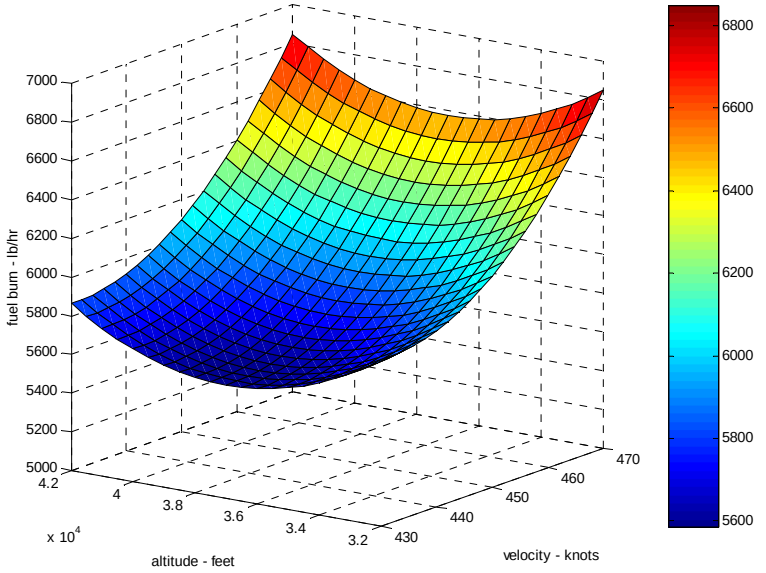

Fig. 7 Quadratic relationship of velocity and altitude with fuel burn

The climb and descent costs, the acceleration cost, and the terminal cost were unchanged from the RH-MILP formulation. The detailed trajectory cost function is given by Eq. (28)

$$J_Q = \left(f_{Q,a}(W) + f_{Q,v}(W) + f_{rc} + A\right)\Delta t - \sum_{i=1}^{N_p} b_{f,i} f_{term,i} \tag{28}$$

where J_Q is the cost, f_{rc} is the vertical velocity cost, A is the acceleration, Δt is the size of the time step, b_f is a binary variable, and f_{term} is the terminal cost.

VI. Example Results

Fuel optimal, and persistent contrail avoiding, trajectories for a flight between Chicago and Los Angeles were found for the RHi field of November 17, 2001. Solutions were found using receding horizon MIQP and MILP, and those results were compared to their respective limiting case (full horizon) solutions. The piecewise linear approximation used in the MILP was analyzed for different numbers of piecewise linear segments. To highlight the differences between MILP and MIQP, limiting case solutions were found for a pathological obstacle field designed to distinguish the characteristics of the quadratic and linear costs. This obstacle field was also used to analyze the sensitivity of the receding horizon controller to changes in planning horizon length and time step size. All of the examples were computed using CPLEX 10.2[32] on a PC laptop with a 2.16GHz Intel Core2 Duo processor and 2GB of RAM.

A. Fuel Optimal Trajectory for Persistent Contrail Avoidance

This example considers a single flight from O'Hare International Airport (ORD) to Los Angeles International Airport (LAX) using atmospheric data from November 17, 2001. The objective of this example was to find a fuel optimal trajectory for this route while flying clear of atmospheric areas containing RHi > 100%. The fuel burn cost was derived from the model presented in Section III, and the formulations of Sections IV and V describe the dynamical and aircraft performance constraints. Table 3 lists the receding horizon parameters and the aircraft performance limitations used in this example.

Table 3 Receding horizon parameters and aircraft performance limits

Number of steps in planning horizon (N_p)	8
Number of steps in the execution horizon (N_e)	4
Time step size (Δt)	3 min
Maximum en-route velocity (V_{max})	470 knots
Minimum en-route velocity (V_{min})	417 knots
Maximum altitude (z_{max})	42,000 ft
Minimum altitude (z_{min})	28,000 ft

Figure 8 shows trajectories overlaid on two-dimensional contour plots of the RHi field at different altitudes. The blue, magenta, and cyan trajectories correspond to RH-MILP formulations, each of which used a different number of piecewise linear segments in the cost function. The black trajectory was optimized with a RH-MIQP formulation, and the red trajectory represents the MILP limiting case formulation, where the goal is contained within the planning horizon. The trajectories were initiated at approximately 34,000 ft, and as seen in Fig. 8b, a region of RHi > 100% over southern Iowa and Missouri forced the trajectories to adjusts their routes. The piecewise linear trajectories followed an almost identical horizontal flight path to avoid contrail formation. The quadratic trajectory deviated from the piecewise linear trajectories, which was caused by a difference in the sensitivity of altitude change to fuel burn in their respective cost functions. The full horizon trajectory followed a much straighter flight path to LAX due to the fact that it was computed in one step and not in a receding horizon fashion.

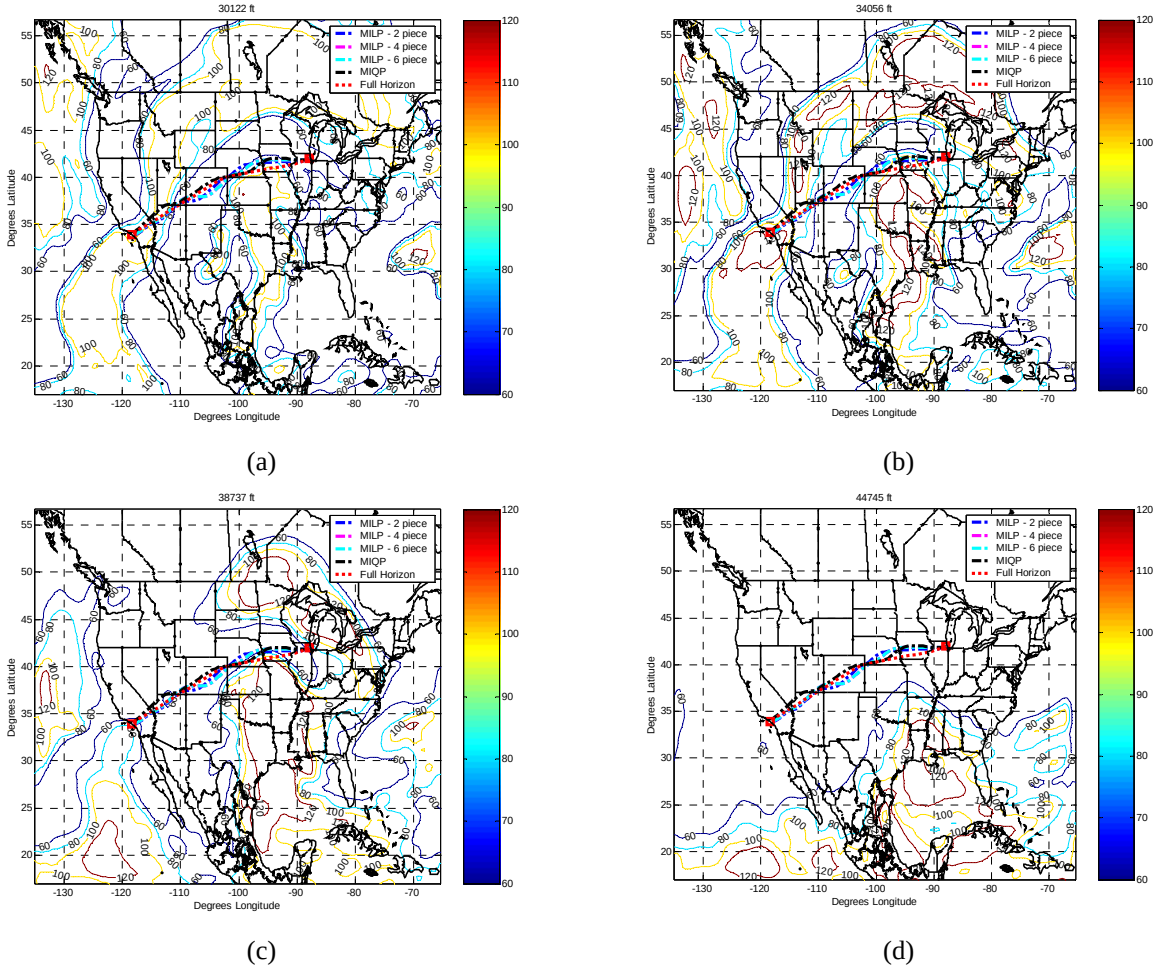

Fig. 8 Fuel optimal trajectories overlaid on contour plots of the RHi field at altitudes of (a) 30122 ft, (b) 34056 ft, (c) 38737 ft, and (d) 44745 ft. A map showing the boundaries of North America is in the background.

Figure 9 shows the aircraft and computational performance associated with the trajectories presented in Fig. 8. Figure 9a shows the velocity profiles of the trajectories, and it is easy to see that the velocities corresponding to the receding horizon formulations are very similar. The difference between the RH-MILPs and the MIQP can, at least in part, be explained by the fact that the MIQP is less sensitive to small velocity variations around the nominal velocity. Figure 9b shows the altitude profiles of the trajectories, where it can be seen that an area of RHi > 100% was encountered approximately 0.4 hours into the flight. The four and six piece RH-MILP trajectories chose to climb over the area, while the two piece RH-MILP, the RH-MIQP, and the full horizon trajectories chose to descend under the area. The climb seen by all trajectories at 2 hours is due to the preprogrammed step-climb profile discussed earlier. Figure 9d shows the computation expense of each method. The two piece RH-MILP was the cheapest, followed by the four and six piece RH-MILPs, and the RH-MIQP was by far the most expensive from a computation standpoint.

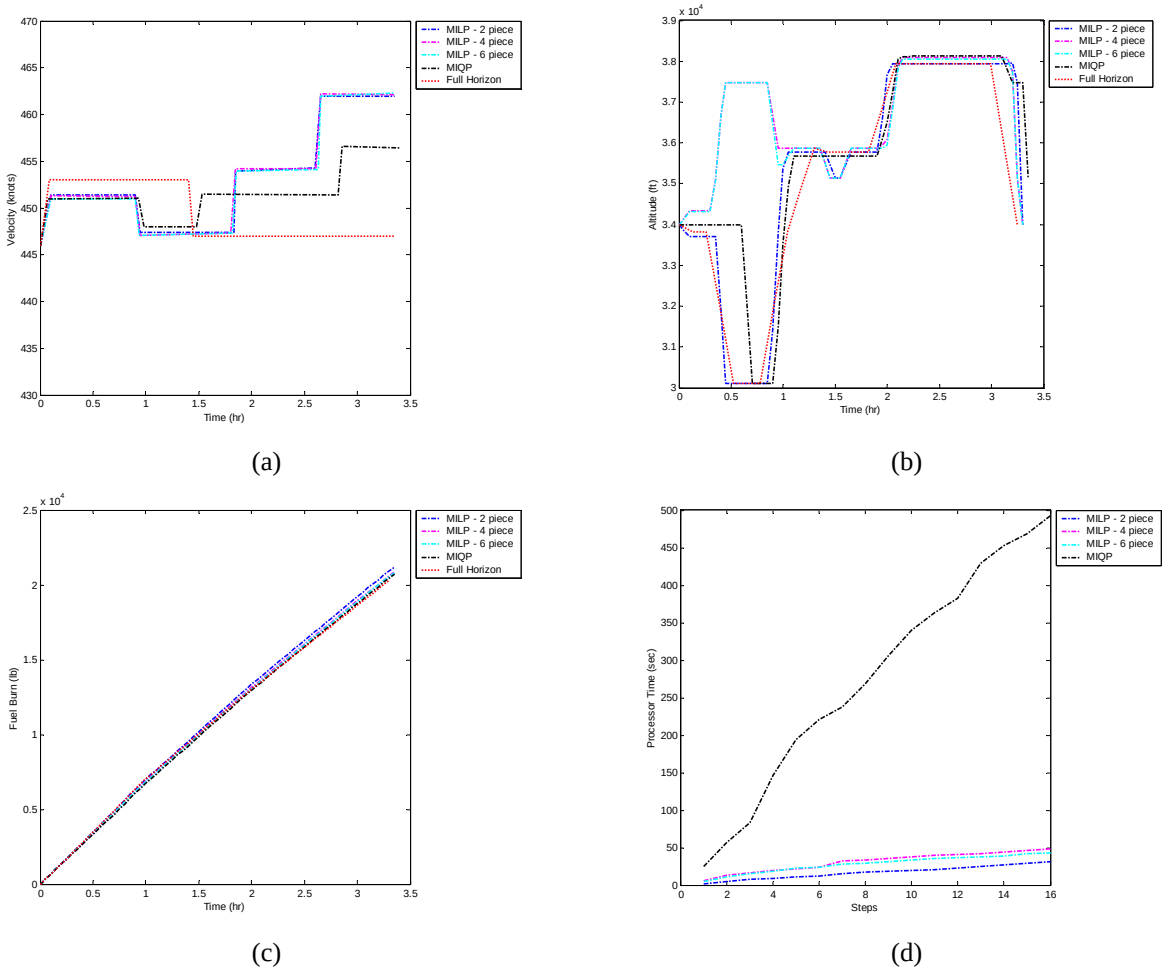

Fig 9. Aircraft and computational performance: (a) velocity time history, (b) altitude time history, (c) fuel burn time history, (d) receding horizon computation time

Table 4 compares the performance of the four trajectories presented by this example. The RH-MIQP showed the best performance in terms of total fuel burn, but was by far the most computationally expensive. The four and six segment RH-MILPs displayed better fuel burn performance than the two segment RH-MILP, and were only slightly more computationally expensive. The receding horizon trajectories burned between 2.88 % and 2.23 % more fuel than the full horizon limiting case. Overall, the full horizon trajectory burned 2.76% more fuel than a trajectory disregarding contrail avoidance.

Table 4 Comparison of receding horizon trajectory performance

	MILP $N_p = 8$, $N_e = 4$ 2 Segment	MILP $N_p = 8$, $N_e = 4$ 4 Segment	MILP $N_p = 8$, $N_e = 4$ 6 Segment	MIQP $N_p = 8$, $N_e = 4$
Max. Velocity	462.3 knots	462.1 knots	462.1 knots	457.3 knots
Avg. Velocity	454.7 knots	454.6 knots	454.6 knots	451.8 knots
Total Fuel Burn	20,824 lbs	20,731 lbs	20,734 lbs	20,695 lbs
% Difference from Full Horizon	2.88 %	2.42 %	2.43 %	2.23 %
Flight Time	3.35 hrs	3.35 hrs	3.35 hrs	3.40 hrs
Max CPU time /step	3.23 sec	8.88 sec	7.27 sec	62.73 sec
Avg CPU time /step	1.94 sec	3.03 sec	2.69 sec	30.83 sec

B. Comparison of MILP and MIQP

A pathological obstacle field was created to exploit the inherent differences between limiting case full horizon MILP and MIQP formulations. Figure 10 shows MILP and MIQP trajectories in this obstacle field. The trajectory created by MILP climbed over the first obstacle, and around the next two, whereas the trajectory created by MIQP climbed over the first obstacle and descended below the next two, making a straight horizontal line to the goal (see Fig. 10a). The MIQP trajectory did this because the quadratic cost is less sensitive to small deviations away from the nominal optimal altitude. On the other hand, the MILP optimization made the decision that descending under obstacles 2 and 3 was more expensive than going around them. Note that it is possible to create a linear approximation to better represent small changes around the nominal, and the MILP would perform better in this scenario. However, that linear approximation would be less sensitive to large deviations from the nominal, so a different pathological scenario could be developed to exploit the shortcomings of the MILP.

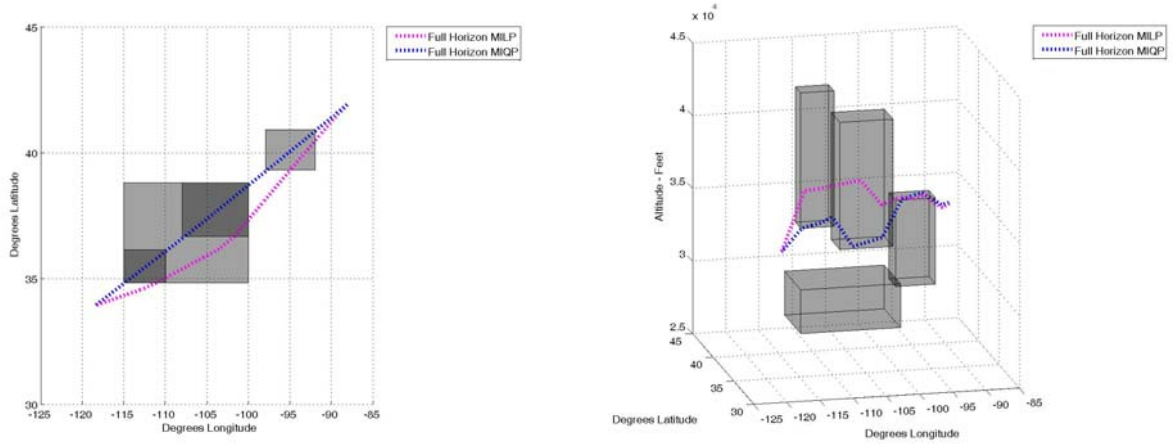

(a) (b)

Fig. 10 Comparison of MIQP and MILP globally optimal trajectories in a pathological obstacle field shown in an (a) overhead view and (b) a three-dimensional view

Figure 11 shows the velocity and altitude time histories for the trajectories of Fig. 10. Notice in the velocity time history that the velocity associated with the MILP increases at about 1.5 hours. This is the time that corresponds to the MILP decision to fly around the obstacles instead of descend under them. The velocity increase corresponds to the longer path length required to reach the goal. Overall, the MILP trajectory burned 0.4% more fuel than the MIQP trajectory.

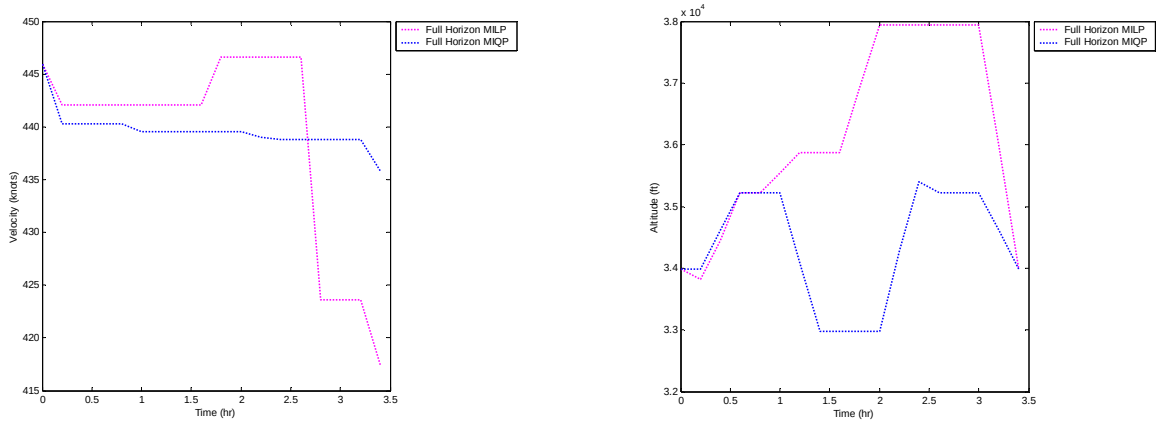

(a) (b)

Fig. 11 Comparison of MIQP and MILP globally optimal aircraft performance in a pathological obstacle field: (a) velocity time history, (b) altitude time history

C. Effect of Planning Horizon Length and Time Step Size

In the receding horizon implementation, the planning horizon length (N_p) and the time step size (Δt) have an effect on the shape of the trajectory. This effect is complicated, but this section will try to isolate the differences and explain possible exceptions to the presented scenarios. The effect of planning horizon was isolated by comparing two trajectories with different planning horizons, but with the same execution horizon and time step. Figure 12 shows the effect of planning horizon in the pathological obstacle field.

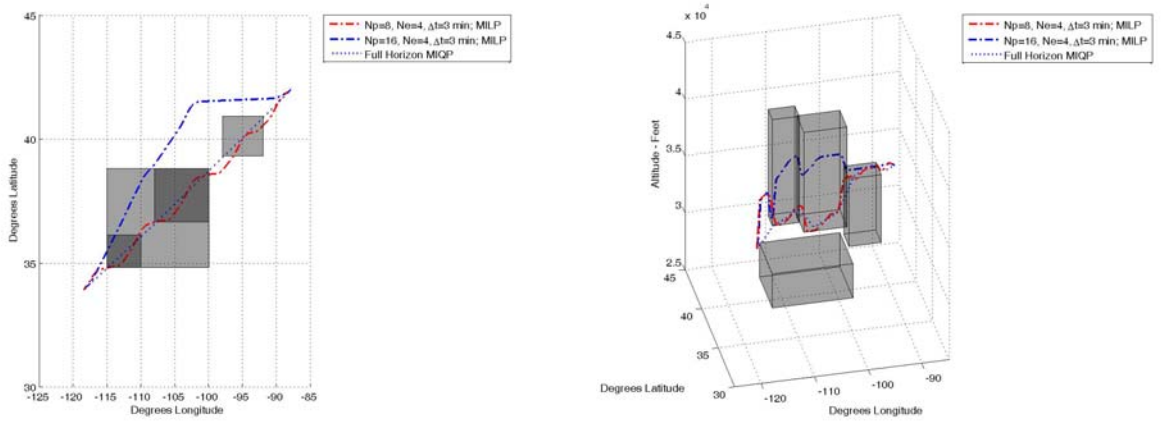

(a) (b)

Fig. 12 Effect of planning horizon length on the receding horizon trajectory

Notice that the trajectory with N_p = 16 is, in general, farther away from the obstacles than the trajectory with N_p = 8. This behavior is caused when the planning horizon is long enough for the trajectory to "peek" around the obstacle during the receding horizon iterations. Essentially, the receding horizon controller moves the detailed trajectory around the obstacle to connect the line of sight with the goal instead of the obstacles along the path. In this case, doubling the length of the planning horizon corresponded to increasing fuel burn by 2.1 %.

The effect of time step size on the receding horizon trajectory is similar to the effect of planning horizon length. Figure 13 shows receding horizon trajectories with time step sizes of 3 min and 6 min in the pathological obstacle field. Notice that the trajectory with Δt = 6 min is farther away from the obstacles. Increasing the size of the time step increases the reachable space in the planning horizon, allowing the trajectory in the planning horizon to "peek" around the obstacles. In this case, doubling the size of the time step corresponded to an increase in fuel burn of 1.8%.

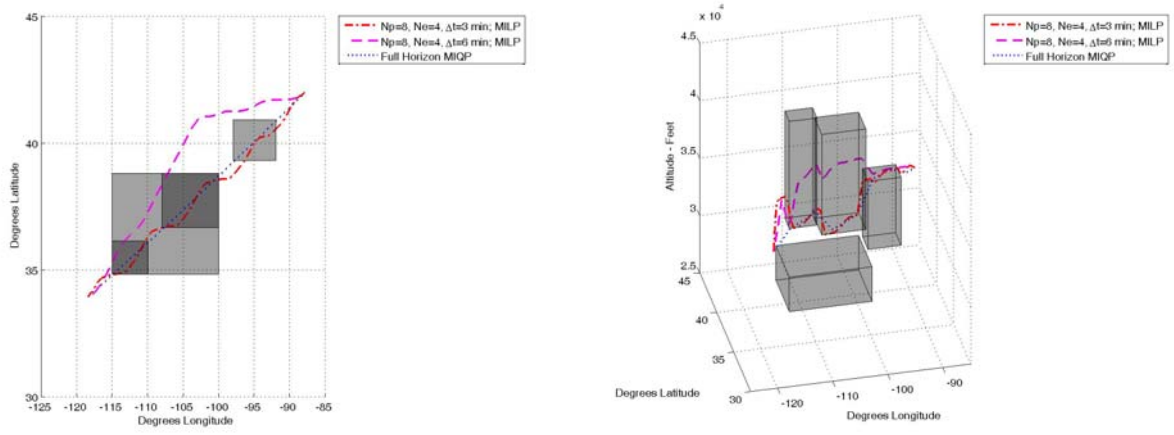

(a) (b)

Fig. 13 Effect of time step size on the receding horizon trajectory

This section presented a couple selected scenarios to explain the effect of planning horizon length and time step size on the shape of a receding horizon trajectory. It is extremely important to note that this behavior is restricted to obstacle fields such as the one presented, which is relatively sparse and scaled appropriately for the contrail problem. A denser obstacle field would decrease the sensitivity to the parameters presented because, most likely, the line of sight to the goal would be blocked by other obstacles, and the apparent benefit of "peeking" would not exist. Also, another important point is that if the planning horizon length or time step size is increased large enough to stretch the reachable space of the planning horizon around the upcoming obstacles, the trajectory will closely match the full horizon solution (think of the limiting case being if the goal is reachable from the initial position). The disadvantage to a planning horizon of this type is that the computational effort is extremely high, which negates the benefit of the receding horizon implementation.

VII. Conclusions

This paper showed the viability of mixed-integer programming as a strategy to optimally reroute aircraft to avoid the formation of persistent contrails. In addition, it analyzed the inherent differences between MILP and MIQP, and investigated the effect of planning horizon length, and time step size on receding horizon trajectory generation. The following specific conclusions were taken from this research:

1. Receding horizon mixed-integer programming is a viable option to optimize aircraft trajectories to avoid persistent contrail formation. For the example scenario considered, the best case contrail avoidance trajectory resulted in a 2.76% increase in fuel burn over a trajectory which did not avoid attempt to avoid contrail formation.
2. While mixed-integer quadratic programming is far more computationally expensive than mixed-integer linear programming, it produced a more efficient trajectory when used in a pathological obstacle field. The viability of MIQP over MILP depends on the required accuracy of solution and the computational demands of the given problem.
3. Within the framework of this problem, the planning horizon length and the time step size had great influence over the solution. This behavior is also dependent on the size of the obstacles in the path of the vehicle. Increasing the length of the planning horizon and the size of the time step had the effect of stretching the trajectory away from the obstacles, and in turn the most efficient solution.

Acknowledgments

The authors would like to thank Marcia Politovich, Frank McDonough, and Gary Cunning of The National Center for Atmospheric Research for their help in obtaining the atmospheric data used in this paper. The work was funded by a Critical Research Initiatives grant from the University of Illinois. The authors would also like to acknowledge the support given to this work by a NASA GSRP fellowship.

References

[1]Waitz, I., Townsend, J., Cutcher-Gershenfeld, J., Greitzer, E., and Kerrebrock, J. *Report to the United States Congress: Aviation and the Environment, A National Vision, Framework for Goals and Recommended Actions*. Partnership for AiR Transportation Noise and Emissions Reduction, MIT, Cambridge, MA, 2004.

[2]Intergovernmental Panel on Climate Change, *Aviation and the Global Atmosphere*. J. E. Penner, D. H. Lister, D. J. Griggs, D. J. Dokken, and M. McFarland (eds.), Cambridge University Press. Cambridge, UK, 1999.

[3]Wuebbles, D, et. al. *Workshop on the Impacts of Aviation on Climate Change: A Report of Findings and Recommendations*. Cambridge, MA, June 7-9, 2006.

[4]Travis, D. J., Carleton, A. M., and Lauritsen, R. G., "Contrails reduce daily temperature range," Nature. Vol 418. 8 August 2002. p. 601.

[5]Next Generation Air Transportation System, Federal Aviation Administration Report to the U.S. Congress, 2004.

[6]Noland, R. B., and Williams, V., "Policies for Mitigating Contrail Formation from Aircraft," *Proceedings of the AAC-Conference*, AAC, Friedrichshafen, June 2003, pp. 328-333.

[7]Williams, V., and Noland, R. B., "Variability of Contrail Formation Conditions and the Implications for Policies to Reduce the Climate Impacts of Aviation," *Transportation Research Part D*, Vol. 10, No. 4, 2005, pp. 169-280.

[8]Fichter, C., Marquart, S., Sausen, R., and Lee, D. S., "The Impact of Cruise Altitude on Contrails and Related Radiative Forcing," *Meteorologische Zeitschrift*, Vol. 14, No. 4, Aug. 2005, pp. 563-572.

[9]Mannstein, H., Spichtinger, P., and Gierens, K., "A Note on How to Avoid Contrail Cirrus," *Transportation Research Part D*, Vol. 10, No. 5, 2005, pp. 421-426.

[10]Klima, K., "Assessment of a Global Contrail Modeling Method and Operational Strategies for Contrail Mitigation," M.S. Thesis, MIT, 2005.

[11]Bryson, A. E., and Ho, Y, C., *Applied Optimal Control*, Taylor and Francis, Levittown, PA, 1975.

[12]Frazzoli, E., "Robust Hybrid Control for Autonomous Vehicle Motion Planning," PhD Dissertation, MIT, 2001.

[13]Milan, M., "Real-Time Optimal Trajectory Generation for Constrained Dynamical Systems," PhD Dissertation, Cal Tech, 2003.

[14]Schouwenaars, T., "Safe Trajectory Planning for Autonomous Vehicles," PhD Dissertation, MIT, 2005.

[15]Kuwata, Y., "Trajectory Planning for Unmanned Vehicles using Robust Receding Horizon Control," PhD Dissertation, MIT, 2007.

[16]Bellingham, J., Richards, A., and How, J. P., "Receding Horizon Control of Autonomous Aerial Vehicles," Proceedings of the IEEE American Control Conference, May 2002, pp. 3741-3746.

[17]Kuwata, Y., and How, J. P., "Three Dimensional Receding Horizon Control for UAVs," Proceedings of the AIAA Guidance, Navigation, and Control Conference, Aug 2004. AIAA-2004-5144.

[18]Culligan, K., "Nap of the Earth Trajectory Design using MILP," M.S. Thesis, MIT, 2006.

[19]Schouwenaars, T., Feron, E., de Moor, B., and How, J. P., "Mixed Integer Programming for Multi-vehicle Path Planning, " Proceedings of the European Control Conference, European Union Control Association, Porto, Portugal, September, 2001, pp. 2603-2608.

[20]Ma, C. S., and Miller, R. H., "Mixed Integer Linear Programming Trajectory Generation for Autonomous Nap-of-the-Earth Flight in a Threat Environment," IEEE Aerospace Conference, 2005.

[21]Chaudhry, A., Misovec, K., and D'Andrea, R., "Low Observability Path Planning for an Unmanned Air Vehicle Using Mixed Integer Linear Programming," *43rd IEEE Conference on Decision and Control*, Paradise Island, Bahamas, Dec. 14-17, 2004.

[22]United States Environmental Protection Agency. "Aircraft Contrails Factsheet," EPA430-F-00-005, September 2000.

[23]Duda et al, "CONUS Contrail Frequency Estimated for RUC and Flight Track Data," European Conference on Aviation, Atmosphere, and Climate, June 30-July 3, 2003.

[24]Benjamin, S. G., D. Devenyi, S. S. Weygandt, K. J. Brundage, J. M. Brown, G. A. Grell, D. Kim, B. E. Schwartz, T. G. Smirnova, T. L. Smith, and G. S. Manikin, "2004: An hourly assimilation/forecast cycle: The RUC," Mon. Wea. Rev., 132, 495-518 (Feb. issue).

[25]Yoder, T., "Development of Aircraft Fuel Burn Modeling Techniques with Applications to Global Emissions Modeling and Assessment of the Benefits of Reduced Vertical Separation Minimums," M.S. Thesis, MIT, 2007.

[26]Jardin, M. R., "Ideal Free Flight through Multiple Aircraft Neighboring Optimal Control," *Proceedings of the American Control Conference*, Chicago, IL, June, 2000, pp. 2879-2885.

[27]Roskam, J., *Airplane Design, Part IV: Preliminary Calculation of Aerodynamic, Thrust and Power Characteristics*, DARcorporation, Lawrence, KS, 2000.

[28]Anderson, J. D., *Aircraft Performance and Design*, McGraw-Hill, 1999.

[29]PERF: Engine Performance Analysis Program v4.2

[30]Lambert, M., Munson, K., Taylor, M, J, H., and Taylor, J. W. R., (eds.) *JANES'S ALL THE WORLD AIRCRAFT*, Jane's Information Group, Alexandria, VA, 1990.

[31]Padilla, C. E., *Optimizing Jet Transport Efficiency*, McGraw-Hill, 1996.

[32]ILOG, *ILOG CPLEX User's guide*, 2007.